Geomechanics and Engineering, *Vol. 36, No. 6 (2024) 563-573*
https://doi.org/10.12989/gae.2024.36.6.563

Investigations of countermeasures used to mitigate tunnel deformations due to adjacent basement excavation in soft clays

Jinhuo Zheng[1], Minglong Shen[1], Shifang Tu[2], Zhibo Chen*[3] and Xiaodong Ni[4]

[1]*Fujian Provincial Institute of Architectural Design And Research Co.,Ltd., Fuzhou 350001, China*
[2]*China Railway 16th Bureau Group 3rd Corporation Limited, Zhejiang Huzhou, 313000, China*
[3]*Department of Geotechnical and Geological Engineering, Zijin School of Geology and Mining, Fuzhou University, Fuzhou 350116, China*
[4]*Key Laboratory of Ministry of Education for Geomechanics and Embankment Engineering, Hohai University, Nanjing, 210024, China*

(*Received November 27, 2023, Revised February 19, 2024, Accepted February 27, 2024*)

Abstract. In this study, various countermeasures used to mitigate tunnel deformations due to nearby multi-propped basement excavation in soft clay are explored by three-dimensional numerical analyses. Field measurements are used to calibrate the numerical model and model parameters. Since concrete slabs can constrain soil and retaining wall movements, tunnel movements reach the maximum value when soils are excavated to the formation level of basement. Deformation shapes of an existing tunnel due to adjacent basement excavation are greatly affected by relative position between tunnel and basement. When the tunnel is located above or far below the formation level of basement, it elongates downward-toward or upward-toward the basement, respectively. It is found that tunnel movements concentrate in a triangular zone with a width of 2 H_e (i.e., final excavation depth) and a depth of 1 D (i.e., tunnel diameter) above or 1 D below the formation level of basement. By increasing retaining wall thickness from 0.4 m to 0.9 m, tunnel movements decrease by up to 56.7%. Moreover, tunnel movements are reduced by up to 80.7% and 61.3%, respectively, when the entire depth and width of soil within basement are reinforced. Installation of isolation wall can greatly reduce tunnel movements due to adjacent basement excavation, especially for tunnel with a shallow burial depth. The effectiveness of isolation wall to reduce tunnel movement is negligible unless the wall reaches the level of tunnel invert.

Keywords: countermeasures; isolation wall; jet grouting; multi-propped basement; tunnel

1. Introduction

To alleviate traffic jams, subway became the most effective transportation tool in mega cities, such as Shanghai, Hong Kong and London. For conveniences of shopping malls and carparks, more and more deep basements were constructed adjacent to existing subway tunnels (e.g., Forth 2004, Leung *et al.* 2000). Because of basement excavation-induced stress changes in the ground, additional movement and stress were caused in existing tunnels, which might affect tunnel serviceability and safety (e.g., Zheng *et al.* 2008, Khabbaz *et al.* 2019, Liang *et al.* 2021, Zaid 2021a, Zaid 2021b, Shi *et al.* 2022).

Currently, many studies have been conducted to investigate deformation mechanisms of existing tunnels due to above or adjacent basement excavation via physical modelling (e.g., Klar *et al*. 2016, Marshall and Mair, 2011, Ng *et al.* 2013, Ng *et al.* 2015, Huang *et al.* 2014, Meng *et al.* 2023, Shi *et al.* 2023) and numerical modelling (e.g., Devriendt *et al.* 2010, Liu *et al.* 2011, Shi *et al.* 2015a, 2019, Li *et al.* 2018, Mahajan *et al.* 2019, Soomro *et al.* 2019, Liu *et al.* 2020, Bu *et al.* 2022). Based on centrifuge model tests, Huang *et al.* (2014) and Zheng *et al.* (2008) found that basement excavation-induced tunnel movements decreased rapidly as an increase in the tunnel cover to diameter ratio (*C/D*). Moreover, Ng *et al.* (2013, 2015) found that tunnel movements due to above basement excavation were much larger than that due to adjacent basement excavation. In those studies, existing tunnels were located far below the formation level of basement. Accordingly, basement excavation had limited negative effects on adjacent tunnels.

In reality, more and more tunnels were located above the formation level of basement, and excessive tunnel movements were induced by basement excavation in soft clays (e.g., Ge 2002, Shi *et al.* 2015b). However, investigations of basement excavation on adjacent tunnels were relatively limited. By conducting three-dimensional analyses of basement-adjacent tunnel interaction, Chen *et al.* (2023) found that tunnel movements at basement centerline became stable when basement length reached 10 H_e (final excavation depth). Ye *et al.* (2021) found that basement excavation-induced deformations in adjacent tunnels were greatly affected by the clear distance between basement and tunnel. By conducting field monitoring, several studies found that tunnel movements due to adjacent and above basement excavations could be more than 60 mm (e.g., Burford 1988, Sharma *et al.* 2001), which heavily

*Corresponding author, Professor
E-mail: cechenzhibo2023@163.com

ISSN: 2005-307X (Print), 2092-6219 (Online)

exceeded the allowable tunnel movement of 10 mm given by Liu *et al.* (2011). Thus, countermeasures were proposed to mitigate tunnel deformations due to basement excavation. Based on field monitoring and numerical analysis, Liu *et al.* (2020) found that the use of micro-disturbance grouting had the ability to effectively correct the deformed tunnel. By installation of reinforced wall between basement and adjacent tunnel, Meng *et al.* (2023) evaluated the effectiveness of reinforced wall on mitigating tunnel deformations. It was found that the use of reinforced wall could slightly decrease tunnel deformation in the vertical direction, but substantially increase tunnel responses in the horizontal direction. It was indicated that the use of reinforced wall could not mitigate tunnel deformations. By conducting extensive numerical analyses, Shi *et al.* (2018) evaluated the effectiveness of countermeasures used to mitigate tunnel deformations due to above basement excavations. It was found that tunnel deformations could be reduced by increasing wall penetration depth, retaining wall and lining thicknesses.

Compared with investigations of tunnel deformation mechanisms due to basement excavation, the effectiveness of countermeasures used to mitigate tunnel deformations was rarely explored, especially for basements excavated at a side of tunnel. In this study, various countermeasures used to alleviate tunnel deformations due to nearby multi-propped basement excavation in Shanghai soft clay were explored by three-dimensional numerical analyses. In practice, countermeasures used to alleviate tunnel responses can be categorized into three groups: (i) soil reinforcement, (ii) tunnel reinforcement and (iii) basement reinforcement. Thus, typical countermeasures, namely soil jet grouting, installation of isolation wall, increase of retaining wall and tunnel lining thickness, were considered in this study. Field measurements were used to calibrate the numerical model and model parameters. The effectiveness of jet grouting, isolation wall, increase of retaining wall and tunnel lining thicknesses on reducing tunnel deformations were analyzed and discussed.

2. Back-analysis of a multi-propped basement excavation in Shanghai soft clay

2.1 Multi-propped basement excavation

Prior to conduct numerical parametric study, responses of a multi-propped basement excavation reported by Ng *et al.* (2012) were used to calibrate soil model and model parameters. This basement was constructed in Shanghai soft clays, which was served as an interchange station of subways. The excavation geometry on plan was approximately rectangular with a length of 149.5 m and a width of 17.6 m. Fig. 1 shows a typical elevation view of the basement with a final excavation depth of 14.5 m. To reduce basement excavation-induced ground soil movements, diaphragm walls with a thickness of 0.6 m and a depth of 26 m were constructed. In total, four horizontal props were installed at 0.4, 3.9, 7.4 and 10.9 m below the ground surface, respectively. The first prop was made of

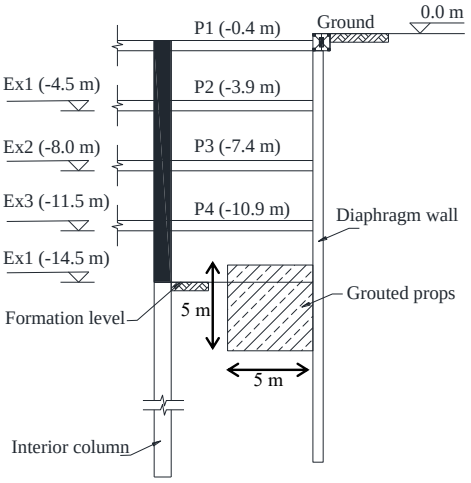

Fig. 1 Typical elevation view of multi-propped basement excavation

concrete with a cross section of 0.6 wide and 0.8 high, while remaining three props were made of steel with an outer diameter of 609 mm and a wall thickness of 16 mm. To reduce basement excavation-induced ground and structure deformations, prestresses of 600, 720 and 700 kN were applied in the three steel props, respectively. For this basement, the vertical spacing of these four props was 3.5 m, while spacings in the horizontal direction were 6 m and 3 m, respectively, for concrete and steel props. Interior columns with a diameter of 1 m and a length of 40 m were installed to support those four props. Inside the basement, soil close to diaphragm wall was reinforced to form 5 m thick grouted props. In this site, instruments were installed to measure basement excavation-induced movements in the diaphragm wall and surrounding soils. All the construction details could be found in Ng *et al.* (2012).

2.2 Soil model and model parameters

The basement excavation was constructed in downtown area of Shanghai, which was located along the southern bank of Yangtze River. Thus, this construction ground was classified as soft stratums, consisting of medium soft clay, soft silty clay, medium clay and medium silty clay. The upper three soft layers were medium soft clay, soft silty clay and medium soft clay with thicknesses of 3.0, 4.5 and 9.0 m, respectively. Below these three soft clays, there were two medium clay and medium silty clay. Extensive laboratory tests were carried out to obtain physical and mechanical properties of these soft and medium clays. Obviously, unit weight, constrained compression modulus and frictional angle had an inverse relationship with water content. In other words, the higher the water content, the lower the unit weight, constrained compression modulus and frictional angle. In this construction site, the constrained compression modulus, cohesion and friction angle were in ranges of 2.3-5.3 MPa, 3.0-11.0 kPa and 26.0-31.0 degree, respectively.

Since shear strains of soil surrounding basement commonly varied from 0.01% to 0.1% (i.e., small strain

Table 1 Physical and mechanical properties of clays in this construction site

Soil Type	Soil Parameter					
	Z m	*w* %	γ kN/m^3	E_s MPa	*C* kPa	φ' °
Medium soft clay	3.0	36.0	18.8	4.0	6.0	29.0
Soft Silty clay	4.5	40.0	17.2	3.2	3.0	27.0
Medium soft clay	9.0	49.0	17.6	2.3	6.0	26.0
Medium clay	13.0	34.0	18.2	3.1	7.0	31.0
Medium silty clay	20.5	25.0	18.4	5.3	11.0	30.0

Table 2 Soil parameters for hardening soil model with small strain stiffness (HSS)

Soil type	Model parameter					
	E_{50}^{ref} MPa	E_{oed}^{ref} MPa	E_{ur}^{ref} MPa	*m*	$\gamma_{0.7}$ 10^{-4}	G_0^{ref} MPa
Medium soft clay	4.5	4.5	27	0.85	2.4	67.5
Soft Silty clay	3.5	3.5	21	0.85	2.5	52.5
Medium soft clay	3	3	18	0.85	2.5	54
Medium clay	3.1	3.1	18.6	0.8	3.2	55.8
Medium silty clay	5.3	5.3	31.8	0.8	3.2	95.4
Grouted prop	15	15	85	0.12	2.0	170

range), soil small-strain stiffness should be considered to gain a better prediction of structure responses due to nearby basement excavation (e.g., Powrie *et al.* 1998, Zheng *et al*. 2018, Ng *et al.* 2015). Thus, advanced constitutive models such as hypoplastic model (HP), hardening soil model with small strain stiffness (HSS) were typically used to analyze soil-structure interaction (e.g., Shi *et al.* 2015a, Shi *et al.* 2019, Zheng *et al.* 2018, Ng *et al*. 2015). According to Plaxis 3D user manual, soil parameters for HSS model could be determined by using compression and triaxial compression shear tests. Thus, the HSS model was adopted to analyze tunnel responses due to nearby basement excavation in Shanghai clay.

For this HSS model, soil responses were mainly controlled by four stiffness parameters (E_{50}^{ref}, E_{oed}^{ref}, E_{ur}^{ref} and G_0^{ref}) and two strength parameters (c, φ'). According to Plaxis 3D user manual and previous studies (e.g., Brinkgreve *et al.* 2004, Zheng *et al.* 2018), these four stiffness parameters had a close relationship with constrained compression stiffness (E_s). In literature, extensive triaxial compression shear tests were conducted to measure the small-strain soil stiffness. It was found that secant modulus (E_{50}^{ref}) and tangent oedometric modulus (E_{oed}^{ref}) was close to constrained compression stiffness (E_s). Moreover, the unloading-reloading modulus (E_{ur}^{ref}) of soft clays was 6 times of the constrained compression stiffness (E_s). For the initial shear modulus (G_0^{ref}), it was 3 times of the unloading-reloading modulus (E_{ur}^{ref}). Based on extensive test results, the modulus stress related power exponent (*m*) was typically in a range of 0.8-1.0 for fine-grained soils. All the soil parameters of HSS model for the soft clay in this construction site were summarized in Table 2.

2.3 Three-dimensional numerical mesh of basement-adjacent tunnel interaction

As introduced in previous section, this basement was served as an interchange station with a very large aspect ratio. Since the length of this cut-and-cover basement was significantly larger than the width, responses of ground and basement were close to plane strain conditions. Thus, only partial basements were simulated in this study to analyze ground, basement and tunnel responses, as shown in Figure 2. To consider the effects of horizontal spacings of concrete and steel props (i.e., 6 m and 3 m), the width of this three-dimensional mesh was 12 m. Moreover, the length and depth of this mesh were 160 m and 60 m, respectively. The clear distance between the retaining wall and the boundary was 71.2 m, which was 4.9 times of the final excavation depth. By analyzing field measurements of basement excavation in soft clays, Hsieh and Ou (1998) found that basement excavation-induced soil deformation zone behind the retaining wall was within four times of the final excavation depth (4 H_e). Obvious, the mesh size designed in this study could suppress the boundary effects on ground and structure responses. As shown in Figs. 2(a) and 2(b), this mesh was used to back-analyze the field study as reported by Ng *et al*. (2012). After validating the numerical model and model parameters, responses of adjacent tunnel due to basement excavation were explored by using the mesh shown in Figs. 2(c) and 2(d). Shell elements were used to simulate diaphragm wall and tunnel, while beam elements were used to model concrete and steel props.

All the soil stratum was simulated by 10 noded tetrahedron elements. Sensitivity analysis was conducted to explore the effects of mesh refinement on ground and structure responses. In total, this three-dimensional mesh of basement-tunnel interaction consisted of 33982 elements and 57394 nodes. By increasing the numbers of nodes and elements by 100%, differences in the maximum tunnel responses were less than 3%. It is indicated that the current mesh density was already fine enough. In order to gain an accurate estimation of tunnel responses, interface elements were applied at soil-structure interfaces. The interface properties were controlled by Mohr-Coulomb failure criterion. In this study, the interface frictional angle was taken as 2/3 of soil interface frictional angle. Soil movements perpendicular to four vertical planes of the mesh were constrained, while soil movements of the bottom plane were restrained in three directions. In this study, consolidation analysis was conducted to obtain long-term responses of adjacent tunnels. Except for top surface of this numerical model, impermeable boundaries were applied to other five surfaces (i.e., front, rear, left, right and bottom surfaces). Construction sequences of this multi-propped basement simulated in the numerical analysis were identical to that in field, as shown in Ng *et al.* (2012).

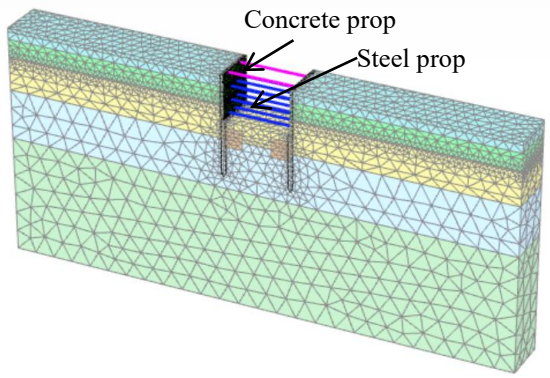

(a) entire mesh of multi-propped basement

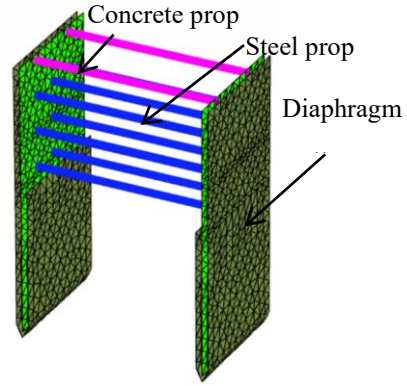

(b) Multi-propped basement

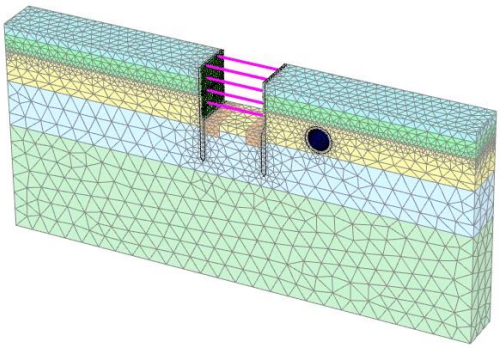

(c) entire mesh of basement-tunnel interaction

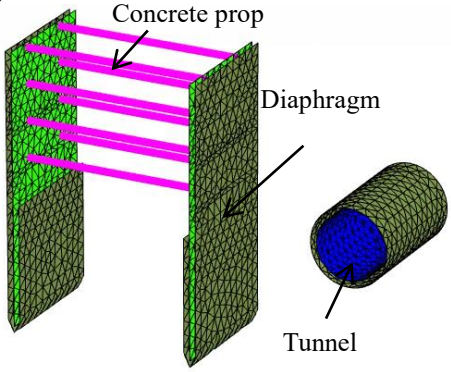

(d) multi-propped basement and tunnel

Fig. 2 Three-dimension numerical mesh of basement-box culvert interaction

2.4 Comparisons of the measured and computed ground and diaphragm wall responses

Fig. 3 compares the measured and computed ground surface soil settlements behind the retaining wall. Negative values represent basement excavation-induced ground soil settlement. The measured ground surface soil settlements at the excavation depth of 8.0 m and 11.5 m are directly compared. Both the measured and computed results show that concave type of ground surface soil settlements are induced behind the retaining wall. This is because the use of diaphragm wall as retaining structure can provide relatively large system stiffness. Because of basement excavation, the measured maximum ground surface soil settlements are 10.3 and 20.3 mm, respectively, when the excavation depths are 8.0 m and 11.5 m. Moreover, the computed ground surface soil settlements at these two excavation depths are 10.2 and 19.3 mm, respectively. Obviously, the maximum difference in the computed and measured maximum ground soil settlements is less than 5%. Generally, the computed ground soil settlements agree well with the measured results. It is indicated that the adopted numerical model and model parameters is reasonable.

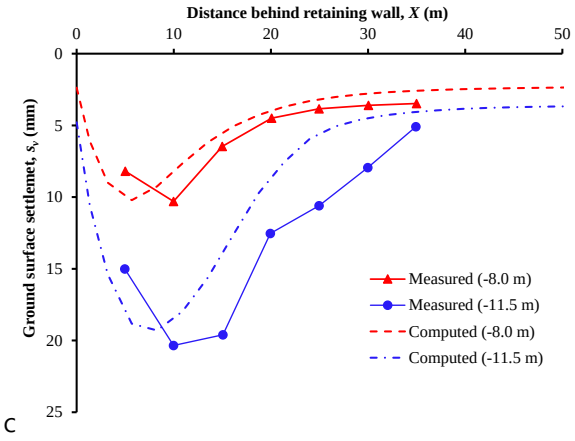

Fig. 3 Comparison of measured and computed ground surface settlement behind retaining wall

Fig. 4 compares the measured and computed lateral wall deflections due to multi-propped basement excavation. Positive values represent retaining wall deforms towards basement. Both the measured and computed results show that a deep-seated deformation mode is observed in the retaining walls. This is because concrete props with a cross section of 0.6 m × 0.8 m are installed at the top of retaining wall, which can effectively constrain lateral movements at the top of the retaining wall. Note that the location of the maximum lateral wall deflection goes deeper as basement excavation proceeds further. As excavation depth increases from 8.0 to 11.5m, the location of the maximum lateral wall deflection varies from 8.9 m to 12.1 m. The retaining walls are constructed into a relatively stiff soil (i.e., medium clay), which can provide relatively high passive resistance to restrain lateral wall movements. Thus, the lateral deflection at the bottom of the retaining wall is suppressed.

When the excavation depths of 8.0 and 11.5 m, the measured maximum lateral wall deflections are 14.6 and 30.1 mm, respectively. Moreover, the computed respective maximum lateral wall deflections at these two excavation depths are 17.7 mm and 30.4 mm, respectively.

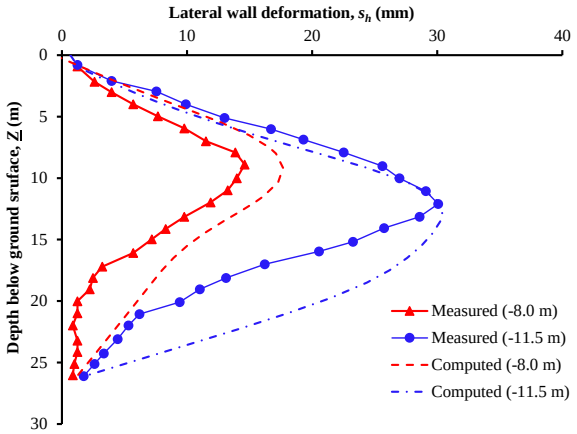

Fig. 4 Comparison of measured and computed deflections of diaphragm wall

Note that there are some discrepancies between the measured and computed results. This is because construction activities, such as traffic load and surcharge around basement are not simulated in the numerical analysis. In general, the measured lateral wall deflections have a good agreement with the computed results, especially for the excavation depth of 11.5 m. It is indicated that again the soil model and model parameters adopted in this study can be used to reasonably estimate structure responses due to basement excavation.

3. Numerical analysis program of basement-tunnel interaction

After verifying numerical model and model parameters, numerical parametric study was carried out to investigate the effectiveness of countermeasures used to alleviate basement excavation-induced tunnel deformations. For a basement excavated at a side of an existing tunnel, tunnel responses were supposed to be affected greatly by retaining wall stiffness, tunnel cover-to-diameter ratio, relative tunnel-basement location. In reality, the shield tunnel was constructed by concrete lining connected by bolts. This study aimed to investigate the effectiveness of countermeasures used to alleviate tunnel responses due to nearby basement excavation, and conclusions drawn from this should not be affected by the tunnel structure. Thus, the shield tunnel was simplified as a continuous structure by applying a reduced flexural stiffness. Table 3 summarized the numerical analysis program conducted in this study. Before incorporating countermeasures, deformation mechanisms of existing tunnel due to adjacent basement excavation were explored. For this scenario, tunnel cover-to-dimeter ratio (*C/D*) and relative basement-tunnel horizontal distance (*H/D*) were designed as 1.0-5.0 and 0.5 to 5.0, respectively. All these designed *C/D* and *H/D* ratios were typical values in practice (Shi *et al*. 2015a, Khabbaz *et al.* 2019, Klar *et al.* 2016).

Four countermeasures, i.e., increase of retaining all and lining thicknesses, jet grouting within basement and installation of isolation wall between retaining wall and tunnel were considered. For tunnel located at the side of basement, tunnel responses were supposed to be significantly affected by lateral wall movements, which was controlled by basement system stiffness. To cover a relatively wide range of basement system stiffness, the thickness of retaining wall varied from 0.4 to 1.2 m. The lower and upper bounds of the designed system stiffness corresponded to flexible and rigid retaining walls. As expected, the increase of passive resistance of soil within basement could also effectively reduce lateral wall movements. In this study, the width of and depth of jet grouting zone below the formation level of basement were considered. Using basement width (B_L) and wall penetration depth (H_p) to normalize the width (B_j) and depth (H_j) of jet grouting zone, the normalized width (B_j/B_L) and depth (H_j/H_p) of jet grouting zone were in ranges of 0.0-1.0 and 0.0-1.0, respectively. By installation of isolation wall between the retaining wall and tunnel, soil movements due to basement excavation could not freely prorogate to adjacent tunnels. To evaluate the effectiveness of isolation wall on reducing tunnel movements, the length of isolation wall varied from 0.0 to 1.0 *H* (i.e., total depth of retaining wall), which was also a typical value in practice (Meng *et al.* 2023). To increase the structure integrity of retaining and isolation walls, rigid connection was applied between those two walls.

Table 3 Numerical analysis program of basement-tunnel interaction

C/D	*H/D*	*T/m*	B_j/B_L	H_j/H_p	*Hi/H*
1.0-5.0	0.5-4.0	0.4 to 1.2	0.0-1.0	0.0-1.0	0.0-1.0

4. Interpretation of tunnel responses due to adjacent multi-propped basement excavation

4.1 Long-term tunnel responses due to multi-propped basement excavation

Fig. 5 shows variations of vertical tunnel movements with construction time. Because of basement excavation, soil stress within basement is significantly smaller than that behind the retaining wall. As expected, tunnel settlement increases rapidly as basement excavation proceeds further. Because of dissipation of excess pore water pressures, soil within basement can be freely expanded if concrete slabs are not cast after soil excavated to the formation level.

Accordingly, tunnel settlements keep increasing with construction time. To suppress long-term tunnel settlement, concrete slabs are cast immediately when soil is excavated to the formation level. Tunnel settlement decreases during construction of concrete slabs and basement structure. This is because basement stiffness increases significantly after casting base and floor slabs. Moreover, the weight of base and floor slabs can compensate stress relief induced by soil removal within basement. Thus, tunnel settlement reaches the maximum value when soil is excavated to the formation level. One thousand days after basement excavation, the maximum tunnel settlements are 30.8 and 4.6 mm,

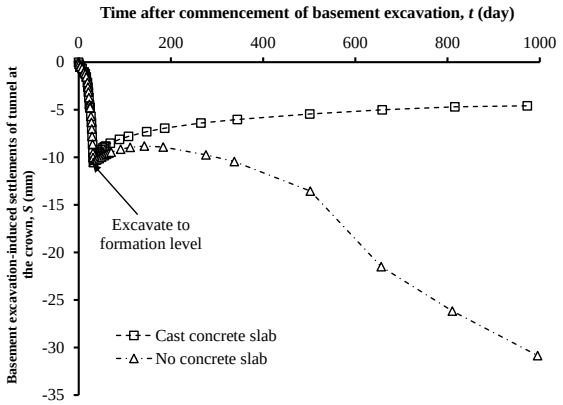

Fig. 5 Variations of tunnel settlement with construction time

respectively for no-casting and casting concrete slabs. Compared the tunnel settlement at the end of basement excavation (i.e., 10.5 mm), no-casting concrete slab can increase tunnel settlement by 193.3%. In reality, concrete slabs and floor slabs are constructed immediately after basement excavation. Because of constraint and counterweight contributed from concrete slabs, the long-term tunnel settlement decreases by 56.2%. Since tunnel settlement reaches the maximum value at the end of soil removal within basement, this settlement is used in following sections.

4.2 Deformation mechanisms of existing tunnel with respect to multi-propped basement excavation

Fig. 6 shows soil displacement vectors and deformed shape of existing tunnel due to basement excavation. Because of soil removal within basement, heave is induced in the soil within basement, while settlement is induced behind the retaining wall. Comparing soil movements at the sides of basement, soil movements surrounding the existing tunnel are much smaller than that at the other side. This is because the existing tunnel has much larger stiffness, which provides shielding effects to effectively reduce soil movements. Accordingly, deformations are induced in the existing tunnel.

As shown in Fig. 6(b), deformed shape of existing tunnel is closely related to the relative position between basement and tunnel. When the existing tunnel is located above the formation level of basement, the existing tunnel elongates downward and toward the basement. In contrary, the existing tunnel elongates upward and toward the basement when the existing tunnel is far below the formation level of basement. For the tunnel located close to the formation level of basement, it only elongates along the horizontal direction. When the normalized clear distance between tunnel and basement (*H/D*) is 0.5, basement excavation-induced resultant tunnel movements are 13.7, 17.4 and 7.2 mm, respectively, for tunnel cover-to-diameter ratios of 1.0, 2.5 and 4.0. By increasing the *H/D* ratio from 0.5 to 2.0, a rapid decrease in the tunnel movements is observed. For tunnel cover-to-diameter ratios of 1.0, 2.5 and

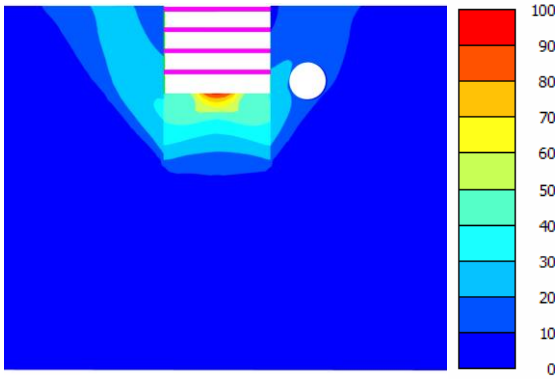

(a) Resultant soil diplacement contor (mm)

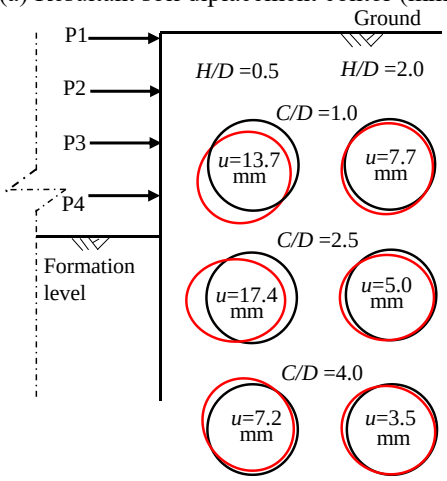

(b) Deformed shape (i.e., enlarged by 200 times)

Fig. 6 Tunnel deformed shape due to basement

4.0, basement excavation-induced resultant tunnel movement decreases to 7.7, 5.0 and 3.5, respectively. Obviously, the resultant tunnel movements decrease by 43.8%-71.3%as the *H/D* ratio from 0.5 to 2.0.

4.3 Effects of relative tunnel-basement location on tunnel responses

As discussed before, tunnel movements are closely related relative positions between the tunnel and basement. Thus, isoline graph of resultant, vertical and horizontal tunnel movements are given in Fig. 7. For tunnel located within 1 H_e from retaining wall, resultant movements of tunnel reach the largest values when the cover depth to tunnel diameter ratio (*C/D*) is 2.0. As the existing tunnel is located far away from the retaining wall (i.e., >2 H_e), the largest movement is observed in the tunnel with a *C/D* ratio of 1.0, as shown in Fig. 7(a). To have a general distribution of tunnel movements at a side of basement, all the tunnel movements are used to plot isoline graphs, as shown in Fig. 7(b). The resultant tunnel movements concentrate in a triangular zone with a maximum width of 2 H_e, especially for tunnel is within 1 H_e away from the retaining wall and located 1 *D* above or 1 *D* below the formation level of basement. Based on the field measurements, Hsieh and Ou (1998) concludes that the major influence zone of basement excavation on soil settlements is within 2 times of the final

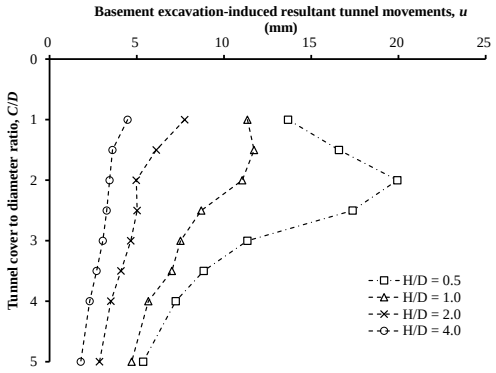

(a) Variation of resultant tunnel movements with depth

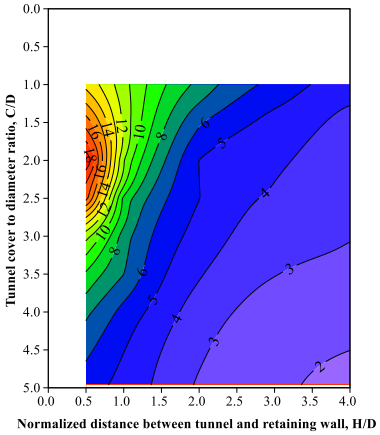

(b) Resultant tunnel movement

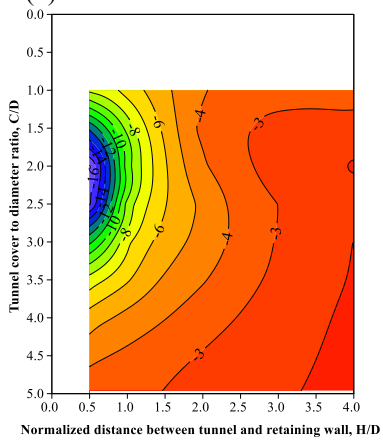

(c) Horizontal tunnel movement

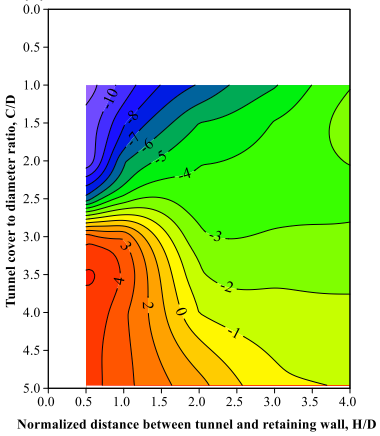

(d) Tunnel settlement

Fig. 7 Isoline graph of tunnel movements due to adjacent basement excavation

excavation depth (H_e). Thus, movements induced in the tunnel are significantly reduced when they are located outside the major influence zone.

Fig. 7(c) shows the distribution of horizontal tunnel movements due to basement excavation. Because of stress relief within basement, the retaining wall deflects toward the basement, as expected. Accordingly, the existing tunnel moves toward the basement. As the tunnel is far away from the basement, the horizontal tunnel movement decreases rapidly. As an increase in the tunnel cover depth, basement excavation-induced horizontal tunnel movements gradually increase to a maximum value, followed by a rapid decrease in the movements. When the tunnel cover depth is close to the final excavation depth (i.e., $C = H_e$), horizontal tunnel movement reaches the largest value. Using tunnel movement of 10 mm as evaluation criteria (Liu *et al.* 2011), the critical tunnel deformation zone is 1 H_e away from the retaining wall and 1 D above or 1 D below the formation level of basement. In the horizontal direction, the existing tunnel always moves to the basement. However, both settlement and heave are induced in the tunnel along the vertical direction. By increasing tunnel cover to diameter ratio, tunnel settlement decreases gradually, and then heave is observed in the tunnel. Obviously, the shallow the tunnel, the large the tunnel settlement. For tunnel located with 2 H_e from the retaining wall, vertical tunnel movement shifts from settlement to heave when the existing tunnel is located 0.8 D below the formation level. Based on those three isoline graphs, movements of tunnel at an arbitrary location can be obtained.

4.4 Effects of retaining wall thickness on tunnel responses

Fig. 8 shows variations of horizontal and vertical tunnel movements with retaining wall thickness. In this section, tunnel cover-to-diameter ratio and normalized distance between tunnel and basement are controlled as 2.0 and 0.5, respectively. Variations of system stiffness of basement ($EI/\gamma_w S^4$) are achieved by changing thickness of retaining walls. To cover a relatively wide range of system stiffness, the thickness of retaining wall varies from 0.4 m to 1.2 m. It is clearly shown that both horizontal and vertical tunnel movements decrease rapidly as an increase in the retaining wall thickness.

When the thickness of retaining wall is 0.4 m, basement excavation-induced horizontal and vertical movements are 41.9 and 24.2 mm, respectively. By increasing the thickness of retaining wall to 0.9 m, the corresponding horizontal and vertical tunnel movements decrease to 18.1 and 11.0 mm, respectively. Obviously, the horizontal and vertical tunnel movements decrease by 56.7% and 54.4%, respectively, by increasing retaining wall thickness from 0.4 to 0.9 m. However, reductions in the tunnel movements are less than 10% by further increasing the retaining wall thickness from 0.9 to 1.2 m, especially for tunnel settlement. Although the use of a thick retaining wall can reduce tunnel movements due to adjacent basement excavation, it is not an economic way to reduce tunnel movements by using a very thick retaining wall.

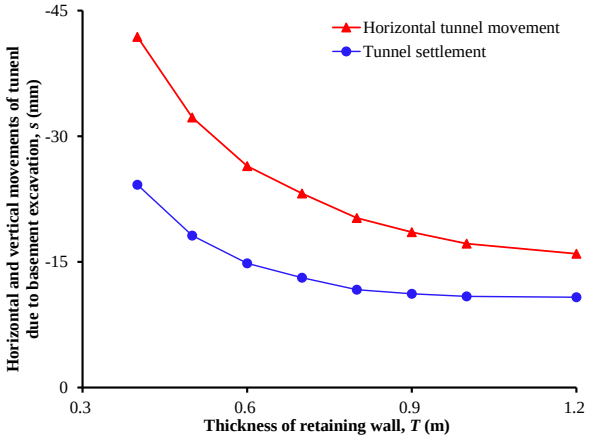

Fig. 8 Effects of retaining wall thickness on tunnel movements

4.5 Effects of jet grouting on tunnel responses

Fig. 9 shows effects of jet grouting on tunnel responses. As expected, tunnel movements are closely related to lateral wall deflection, which is greatly affected by passive resistance of soil within basement. The normalized depth of jet grouting (H_j/H_p) varies from 0 (i.e., no jet grouting) to 1.0 (i.e., depth of jet grouting zone is equal to wall penetration depth). In this case, the width of jet grouting zone is 5 m. As an increase in the jet grouting depth, soil passive resistances used to restrain lateral wall movement increase as well. Moreover, the reinforcement of soil within basement can restrain soil sliding from outside to basement. Accordingly, basement excavation-induced horizontal and vertical tunnel movements decrease rapidly, especially for tunnel settlement. When there is no any jet grouting, basement excavation-induced maximum tunnel settlement and horizontal movement are 16.0 and 20.8 mm, respectively. When the soil is reinforced to the bottom of the retaining wall, the respective settlement and horizontal movement of tunnel decrease to 3.1 and 11.1 mm. Obviously, soil reinforcement within basement can decease settlement and horizontal movement of tunnel decrease by 80.7% and 46.7%, respectively.

Compared with soft soil, grouted soil can be classified as grouted props. Thus, responses of basement and tunnel are expected to be affected by the width of the grouted props. The normalized width of grouted prop (B_j/B_p) varies from 0 (i.e., no jet grouting) to 1.0 (i.e., jet grouting along the entire width). In this case, the thickness of jet grouting zone is 5 m. As an increase in the width of the grouted prop, basement excavation-induced tunnel movements decrease rapidly. By increasing the normalized width of grouted prop from 0.0 to 1.0, the settlement and horizontal movement of existing tunnel decrease by 61.3% and 48.3%, respectively. Obviously, jet grouting of soil within basement can greatly reduce tunnel deformations due to adjacent basement excavation. Thus, the use of jet grouting within basement is the most effective countermeasure to reduce tunnel responses due to basement excavation.

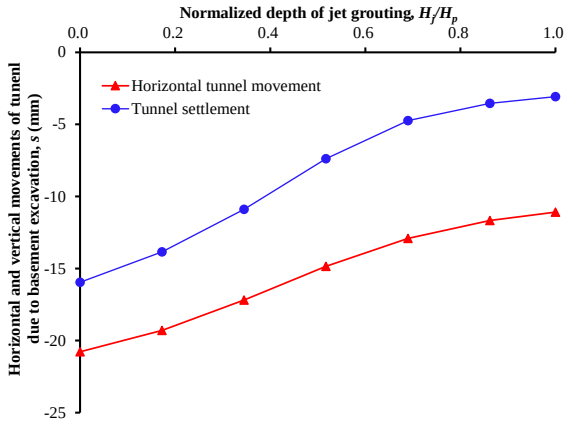

(a) Effects of jet grouting depth

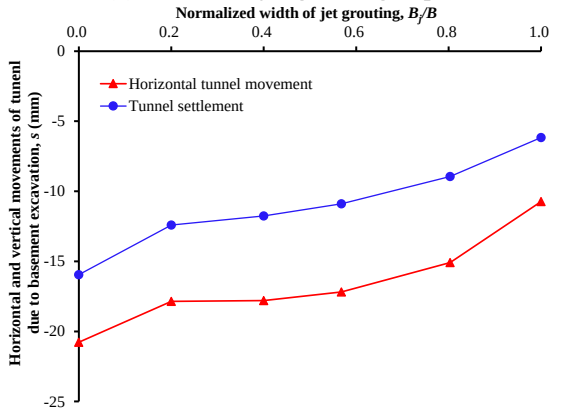

(b) Effects of jet grouting width

Fig. 9 Effects of jet grouting on tunnel movements due to nearby basement excavation

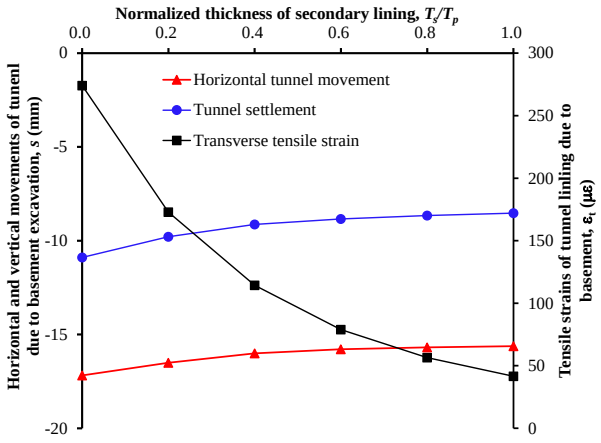

Fig. 10 Effects of secondary lining thickness on basement excavation-induced tunnel movements

4.6 Effects of lining thickness on tunnel responses

Fig. 10 shows basement excavation-induced tunnel movements under various thicknesses of secondary lining (T_s), which is normalized by the thickness of primary lining (T_p). Obviously, the flexural stiffness of tunnel lining increases rapidly an increase in the thickness of secondary lining. Accordingly, the maximum tensile strain induced in

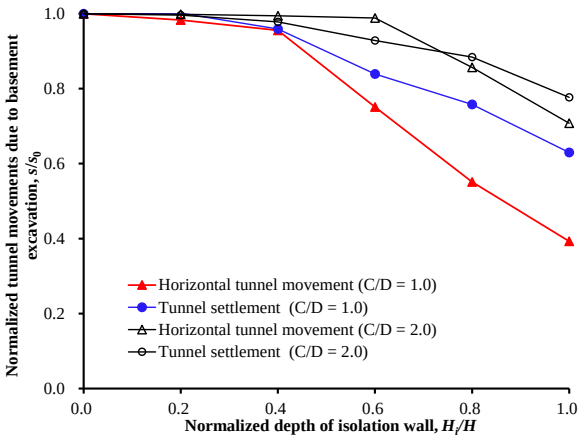

Fig. 11 Effects of isolation wall depth on basement excavation-induced tunnel movements

the lining decreases from 274.1 με to 41.6 με as the normalized lining thickness varies from 0.0 to 1.0. However, effects of lining thickness on tunnel movements are limited. Under the same variation of lining thickness, the horizontal movement and settlement of the existing tunnel only reduce by 9.1% and 21.7%, respectively. For a basement excavated at a side of tunnel, tunnel deformations are controlled by translational movement and distortion. By using a thick lining, distortion of tunnel lining can be dramatically reduced, but reductions in the tunnel movements are limited. It is indicated that deformations of tunnel lining at a side of basement are dominated by its translational movements.

4.7 Effects of installation of isolation wall on tunnel responses

Fig. 11 shows basement excavation-induced tunnel movements under various depth of isolation wall (H_i), which is normalized by the depth of retaining wall (H). Obviously, tunnel movements are almost independent of isolation wall if its depth is small. However, tunnel movements can be reduced dramatically by using a very deep isolation wall. When depth of isolation wall is the same as the retaining wall, horizontal movement and settlement of a deep tunnel (i.e., C/D =2.0) decrease by 29.2% and 22.3%, respectively. However, reductions of horizontal movement and settlement in a shallow tunnel (i.e., C/D =1.0) 39.3% and 63.0%, respectively. Obviously, movements of shallowly buried tunnel can be more effectively reduced by installation of isolation wall. When the tunnel cover to diameter ratio (C/D) is 2.0, a rapid decrease in the tunnel movements is observed as the normalized depth of isolation wall reaches 0.8 (i.e., 20.8 m). For a shallowly buried tunnel (i.e., C/D = 1.0), tunnel movements decreases rapidly when the normalized depth of isolation wall is larger than 0.4 (i.e., 10.4 m). It is indicated that the effectiveness of using isolation wall to reduce tunnel movement is negligible unless the isolation wall reaches the invert of tunnel lining.

5. Conclusions

In this study, various countermeasures used to mitigate tunnel deformations due to nearby multi-propped basement excavation in Shanghai soft clay are explored by three-dimensional numerical analyses. Field measurements are used to calibrate the numerical model and model parameters. Based on the computed results, the following conclusions may be drawn:

• Because of basement excavation-induced stress relief, tunnel movements increase rapidly as basement excavation proceeds further. However, tunnel movements are suppressed after casting concrete slabs. Thus, tunnel movements reach the maximum values when soils are excavated to the formation level of basement.

• Deformation shapes of an existing tunnel due to adjacent basement excavation are greatly affected by relative position between tunnel and basement. When the tunnel is located above or far below the formation level of basement, it elongates downward-toward or upward-toward the basement, respectively. However, the tunnel only elongates horizontally when it is located close to the formation level.

• Deformation contours used to estimate tunnel movements is developed. It is found that tunnel movements concentrate in a triangular zone with a width of 2 H_e and a depth of 1 D above or 1 D below the formation level of basement.

• By increasing retaining wall thickness from 0.4 m to 0.9 m, tunnel movements decrease by up to 56.7%. However, reductions in the tunnel movements are less than 10% by further increasing the retaining wall thickness from 0.9 to 1.2 m.

• Jet grouting of soil within basement can effectively reduce basement excavation-induced tunnel movements. Tunnel movements can be reduced by as high as 80.7% and 61.3%, respectively, when the entire depth and width of soil within basement are reinforced.

• For a basement excavated at a side of tunnel, tunnel deformations are controlled by translational movement and distortion. By increasing lining thickness by 100%, basement excavation-induced tensile strain of tunnel can be reduced by up to 78.5%, but reduction of the tunnel movements is less than 21.7%. It is indicated that deformations of tunnel lining at a side of basement are dominated by its translational movements.

• By installation of isolation wall with the same depth of retaining wall, reduction in the movements of deep (C/D =2.0) and shallow (C/D =1.0) tunnels is up to 29.2% and 63.0%, respectively. Obviously, movements of shallow tunnel can be more effectively reduced by installation of isolation wall. It is also found that the effectiveness of using isolation wall to reduce tunnel movement is negligible unless the isolation wall reaches the invert of tunnel lining. The conclusions drawn from this study can be applied to soft ground. Attentions should be paid when applying these conclusions to different ground conditions.

Acknowledgments

This work described in this paper is supported by a research grant from Housing and Urban-rural Development of Fujian, China (Grant No. 2022-K-330), and National

Natural Science Foundation of China (Grant No. 52278335).

References

Brinkgreve, R.B.J. and Broere, W. (2004), PLAXIS 3D Tunnel Version 2, PLAXIS by, Netherlands.

Burford, D. (1988), "Heave of tunnels beneath the shell centre", London, 1959-1986. *Géotechnique*, **38**(1), 135-137.

Bu, F.M., Yu, W.R., Chen, L. and Wu, E.R. (2022), "Investigation of three-dimensional deformation mechanisms of box culvert due to adjacent deep basement excavation in clays", *Geomech. Eng.*, **30**(6), 565-577. https://doi.org/10.12989/gae.2022.30.6.565.

Chen, W.C., Tang, L.X., Zhao, H.J., Yin, Q., Dong, S., Liu, J., Zhu, Z.H. and Ni, X.D. (2023), "Investigation of three-dimensional deformation mechanisms of existing tunnels due to nearby basement excavation in soft clay", *Geomech. Eng.*, **34**(2), 115-124. https://doi.org/10.12989/gae.2023.34.2.115.

Devriendt, M., Doughty, L., Morrison, P. and Pillai, A. (2010), "Displacement of tunnels from a basement excavation in London", *Proceedings of the Institution of Civil Engineers-Geotechnical Engineering*, **163**(3), 131-145. https://doi.org/10.1680/geng.2010.163.3.131.

Forth, R.A. (2004), "Groundwater and geotechnical aspects of deep excavations in Hong Kong", *Eng. Geol.*, **72**(3-4), 253-260. https://doi.org/ 10.1016/j.enggeo.2003.09.003.

Ge, X.W. (2002). Response of a shield-driven tunnel to deep excavations in soft clay. Ph.D thesis, Department of Civil and Environmental Engineering, The University of Hong Kong Science and Technology, HKSAR.

Hsieh, P.G. and Ou, C.Y. (1998), "Shape of ground surface settlement profiles caused by excavation", *Can. Geotech. J.*, **35**(6), 1004-1017. https://doi.org//10.1139/cgj-35-6-1004.

Huang, X., Huang, H.W. and Zhang, D.M. (2014), "Centrifuge modelling of deep excavation over existing tunnels", *Proceedings of the ICE-Geotechnical Engineering*, **16**(2), 3-18. https://doi-org/10.1680/geng.11.00045.

Khabbaz, H., Gibson, R. and Fatahi, B. (2019), "Effect of constructing twin tunnels under a building supported by pile foundations in the Sydney central business district", *Underground Sp.*, **4**(4), 261-276. https://doi.org/10.1016/j.undsp.2019.03.008.

Klar, A., Elkayam, I. and Marshall, A.M. (2016), "Design oriented linear equivalent approach for evaluating the effect of tunneling on pipelines", *J. Geotech. Geoenviron. Eng.*, **142**(1), 04015062. https://doi.org/10.1061/(ASCE)GT.1943-5606.0001376.

Leung, C.F., Chow, Y.K. and Shen, R.F. (2000), "Behavior of pile subject to excavation-induced soil movement", *J. Geotech. Geoenviron. Eng.*, **126**(11), 947-954. https://doi.org/10.1061/(ASCE)1090-0241(2000)126:11(947).

Li, C.W., Li, W. and Liang, Z.R. (2018), "Design and analysis on synchronous construction of deep foundation pit on both sides of tunnels in soft soils", *Chinese J. Undergr. Sp. Eng.*, **14**(S1), 197-203. https://doi.org/10.16285/j.upe.2018.S1.031.

Liang, R.C., Wu, J., Sun, L.W., Shen, W. and Wu, W.B. (2021), "Performances of adjacent metro structures due to zoned excavation of a large-scale basement in soft ground", *Tunn. Undergr. Sp. Tech.*, **117**, 104123. https://doi.org/10.1016/j.tust.2021.104123.

Liu, B., Zhang, D.W., Yang, C. and Zhang, Q.B. (2020), "Long-term performance of metro tunnels induced by adjacent large deep excavation and protective measures in Nanjing silty clay", *Tunn. Undergr. Sp. Tech.*, **95**, 103147. https://doi.org/10.1016/j.tust.2019.103147.

Liu, H.L., Li, P. and Liu, J.Y. (2011), "Numerical investigation of underlying tunnel heave during a new tunnel construction", *Tunn. Undergr. Sp. Tech.*, **26**(2), 276-283. https://doi.org/org/10.1016/ j.tust.2010.10.002.

Mahajan, S., Ayothiraman, R. and Sharma, K.G. (2019), "A parametric study on effects of basement excavation and foundation loading on underground metro tunnel in soil", *Indian Geotech. J.l*, **49**, 667-686. https://doi.org/10.1007/s40098-019-00361-x.

Marshall, A.M. and Mair, R.J. (2011), "Tunneling beneath driven or jacked end-bearing piles in sand", *Can. Geotech. J.*, **48**(12), 1757-1771. https://doi.org/10.1139/t11-067.

Meng, F.Y., Chen, R.P., Liu, Y., Wu, H.N. and Cheng, H.Z. (2023), "Impacts of reinforced wall on nearby excavation-induced ground and tunnel responses: a centrifugal and numerical study", *Tunn. Undergr. Sp. Tech.*, **132**, 104903. https://doi.org/10.1016/j.tust.2022.104903.

Ng, C.W.W, Hong, Y., Liu, G.B. and Liu, T. (2012), "Ground deformations and soil-structure interaction of a multi-propped excavation in Shanghai soft clay", *Géotechnique*, **62**(10), 907-921. https://doi.org/10.1680/geot.10.P.072.

Ng, C.W.W, Shi, J.W. and Hong, Y. (2013), "Three-dimensional centrifuge modelling of basement excavation effects on an existing tunnel in dry sand", *Cana. Geotech. J.*, **50**(8), 874-888. https://doi.org/10.1139/cgj-2012-0423.

Ng, C.W.W., Shi, J.W., Mašín, D., Sun, H.S. and Lei, G.H. (2015), "Influence of sand density and retaining wall stiffness on the three-dimensional responses of a tunnel to basement excavation", *Can. Geotech. J.*, **52**(8), 1811-1829. https://doi.org/10.1139/ cgj-2014-0150.

Powrie, W., Pantelidou, H. and Stallebrass, S.E. (1998), "Soil stiffness in stress paths relevant to diaphragm walls in clay", *Géotechnique*, **48**(4), 483-494. https://doi.org/10.1680/geot.1998.48.4.483.

Sharma, J.S., Hefny, A.M., Zhao, J. and Chan, C.W. (2001), "Effect of large excavation on displacement of adjacent MRT tunnels", *Tunn. Undergr. Sp. Tech.*, **16**(2), 93-98. https://10.1016/S0886-7798(01)00033-5.

Shi, J.W., Chen Y.H., Lu, H., Ma, S.K. and Ng, C.W.W. (2022), "Centrifuge modeling of the influence of joint stiffness on pipeline response to underneath tunnel excavation", *Can. Geotech. J.*, **59**(9), 1568-1586. https://10.1139/cgj-2020-03601.

Shi, J.W., Fu, Z.Z. and Guo, W.L. (2019), "Investigation of geometric effects on three-dimensional tunnel deformation mechanisms due to basement excavation", *Comput. Geotech.*, **106**, 108-116. https://doi.org/10.1016/j.compgeo.2018.10.019.

Shi, J.W., Liu, G.B., Huang, P. and Ng, C.W.W. (2015b), "Interaction between a large-scale triangular excavation and adjacent structures in Shanghai soft clay", *Tunn. Undergr. Sp. Tech.*, **50**, 282-295. https://doi.org/10.1016/j.tust.2015.07.013.

Shi, J.W., Ng, C.W.W. and Chen, Y.H. (2015a), "Three-dimensional numerical parametric study of the influence of basement excavation on existing tunnel", *Comput. Geotech.*, **63**, 146-158. https://doi.org/10.1016/j.compgeo.2014.09.002.

Shi, J.W., Wang, J.P., Chen Y.H., Shi, C., Lu, H., Ma, S.K. and Fan, Y.B. (2023), "Physical modeling of the influence of tunnel active face instability on existing pipelines", *Tunn. Undergr. Sp. Tech.*, **140**, 105281. https://10.1016/j.tust.2023.105281.

Shi, J.W., Zhang, X., Chen, Y.H. and Chen, L. (2018), "Numerical parametric study of countermeasures to alleviate basement excavation effects on an existing tunnel", *Tunn. Undergr. Sp. Tech*., **72**, 145-153. https://10.1016/j.tust.2017.11.030.

Soomro, M.A., Saand, A., Mangi, N., Mangnejo, D.A., Karira, H. and Liu, K. (2019), "Numerical modelling of effects of different multipropped excavation depths on adjacent single piles: comparison between floating and end-bearing pile responses",

Eur. J. Environ. Civil Eng., **25**(14), 2592-2622. https://doi.org/10.1080/19648189.2019.1638312.

Ye, S.H., Zhao, Z.F. and Wang, D.Q. (2021), "Deformation analysis and safety assessment of existing metro tunnels affected by excavation of a foundation pit", *Undergr. Sp.*, **6**, 4211-431. https://doi.org/10.1016/j.undsp. 2020.06.002.

Zaid, M. (2021a), "Three-dimensional finite element analysis of urban rock tunnel under static loading condition: effect of the rock weathering", *Geomech. Eng.*, **25**(2), 99-109. https://doi.org/10.12989/gae.2021.25.2.099.

Zaid, M. (2021b), "Preliminary study to understand the effect of impact loading and rock weathering in tunnel constructed in quartzite", *Geotech. Geol. Eng.*, **42**, 725–753. https://doi.org/10.1007/s10706-021-01948-z.

Zheng, G. and Wei, S.W. (2008), "Numerical analysis of influence of overlying pit excavation on existing tunnels", *J. Central South Univ. Tech.*, **15**(2), 69-75. https://doi.org/10.1007/s11771-008-0438-4.

Zheng, G., Yang, X.Y., Zhou, H.Z., Du, Y.M., Sun, J.Y. and Yu, X.X. (2018), "A simplified prediction method for evaluating tunnel displacement induced by laterally adjacent excavations", *Comput. Geotech.*, **95**, 119-128. https://doi.org/10.1016/j.compgeo.2017.10.006.

GC